

Transition to the Haldane phase driven by electron-electron correlations

A. Jażdżewska,¹ M. Mierzejewski,² M. Środa,² A. Nocera,³ G. Alvarez,⁴ E. Dagotto,^{5,6} and J. Herbrych^{2,*}

¹*Faculty of Physics and Astronomy, University of Wrocław, 50-383 Wrocław, Poland*

²*Institute of Theoretical Physics, Wrocław University of Science and Technology, 50-370 Wrocław, Poland*

³*Department of Physics and Astronomy and Stewart Blusson Quantum Matter Institute, University of British Columbia, Vancouver, B.C. V6T 1Z1, Canada*

⁴*Computational Sciences and Engineering Division, Oak Ridge National Laboratory, Oak Ridge, Tennessee 37831, USA*

⁵*Department of Physics and Astronomy, University of Tennessee, Knoxville, Tennessee 37996, USA*

⁶*Materials Science and Technology Division, Oak Ridge National Laboratory, Oak Ridge, Tennessee 37831, USA*

One of the most famous quantum systems with topological properties, the spin $S = 1$ antiferromagnetic Heisenberg chain, is well-known to display exotic $S = 1/2$ edge states. However, this spin model has not been analyzed from the more general perspective of strongly correlated systems varying the electron-electron interaction strength. Here, we report the investigation of the emergence of the Haldane edge in a system of interacting electrons – the two-orbital Hubbard model – with increasing repulsion strength U and Hund interaction J_H . We show that interactions not only form the magnetic moments but also form a topologically nontrivial fermionic many-body ground-state with zero-energy edge states. Specifically, upon increasing the strength of the Hubbard repulsion and Hund exchange, we identify a sharp transition point separating topologically trivial and nontrivial ground-states. Surprisingly, such a behaviour appears already at rather small values of the interaction, in a regime where the magnetic moments are barely developed.

Introduction

The precise role of the electron-electron interaction in many condensed matter systems is still under much debate. From the high critical temperature superconductivity of copper- and iron-based compounds to the magnetic properties of idealized spin models, strong correlations appear crucial for our understanding of materials physics. In parallel, topology in various compounds has been typically realized and investigated at the level of non-interacting band structures in the presence of spin-orbit coupling. However, the detailed study of the Coulomb correlation effects intertwined with topological physics has barely started and represents one of the grand challenges of present-day theoretical and experimental physics.

In particular, in one of the most famous topologically nontrivial systems, i.e., the $S = 1$ antiferromagnetic (AFM) Heisenberg model $H_S = J \sum_{\ell} \mathbf{S}_{\ell} \cdot \mathbf{S}_{\ell+1}$ on a one-

dimensional (1D) lattice geometry, the spin-spin interactions are necessary to form the zero-energy edge states, which is the hallmark of topological states. In his seminal work [1, 2], Haldane showed that integer $S = 1, 2, \dots$ and half-integer $S = 1/2, 3/2, \dots$ spin systems behave fundamentally different: the former are gapped while the latter are gapless. Affleck, Kennedy, Lieb, and Tasaki (AKLT) proved [3] that the ground-state of $S = 1$ chains, when generalized including biquadratic interactions, can be expressed as a valence bond state (VBS) composed of interacting $S = 1/2$ -like singlets. In this picture, the AKLT state, when defined on an open chain, has two unpaired $S = 1/2$ spins at the edges of the system, forming zero-energy modes.

The existence of topologically protected edge states in $S = 1$ chains has been shown by extensive theoretical [4–7] and experimental [8–13] studies. Also, the road to the Haldane states from well-formed $S = 1/2$ spins has been studied. The AKLT VBS state initiated various investigations of extended Bose Hubbard model (containing nearest-neighbour interactions) [14, 15] and ladder-like $S = 1/2$ systems [16–18]. In the latter, the topological $S = 1$ Haldane phase is a consequence of competition between various kinetic terms (i.e., ferromagnetic rung exchange or AFM frustration) or unpaired sites at the edges of overall AFM systems. Although such systems are fruitful playground for theoretical investigations and even are realized in cold atoms in optical lattice setups [11], they don't fully capture the physics of solid-state compounds. In real low-dimensional materials [19], the $S = 1$ moments should arise due to the electron-electron correlations in a multi-orbital Hubbard model setup, which is technically challenging. Because the $S = 1/2$ moments themselves are already an effective description of some fermionic systems, such analysis is usually unnecessary for many compounds. But in more refined descriptions, the Coulomb repulsion and Hund's coupling not only cooperate but also can compete [20, 21]. Depending on their specific values, the Mott localization of electrons and the formation of well-developed spins can occur in portions of the phase diagram. As an example, in the largest family of $S = 1$ chains, the nickel-based compounds [19], the two e_g electrons of Ni^{+2} ions are necessary to form the $S = 1$ spins due to the Hund's rule that maximizes the on-site magnetic moment. For AgVP_2S_6

* jacek.herbrych@pwr.edu.pl

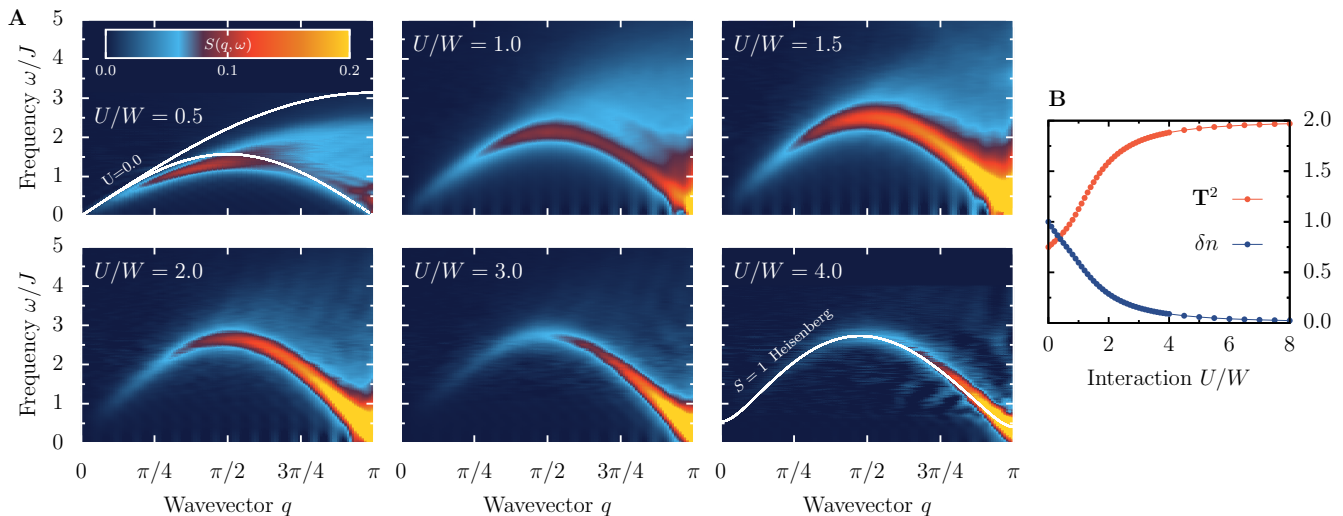


Figure 1. **Spin excitations.** **A** Evolution of the spin excitations, as measured by the dynamical spin structure factor $S(q, \omega)$, with increasing strength of electron-electron interaction U for a system of $L = 80$ sites and $J_H/U = 0.25$. The frequency scale was renormalized by the effective spin exchange $J = 2t^2/(U + J_H)$. White lines in the left top panel represent the two-spinon continuum of the $U = 0$ Hubbard model, while the line in the bottom right panel depicts the magnon dispersion of the $S = 1$ Heisenberg model. In the open boundary systems considered here, the zero energy Haldane edge states are expected at $\omega = 0$. However, the large intensity of these modes can blur the spectra's details. To avoid this issue, we have evaluated the spin excitations only in the bulk of the system (see Methods). **B** Total magnetic moment per site $\mathbf{T}^2 = \mathcal{S}(\mathcal{S} + 1)$ and charge fluctuations δn vs. interaction strength U . Note \mathbf{T}^2 starts at 0.75 for noninteracting $U = 0$ electrons.

or $\text{Ti}_2\text{Ru}_2\text{O}_7$, the $\mathcal{S} = 1$ spins develop, instead, on the t_{2g} orbitals of V^{+3} or Ru^{+4} , respectively. In all the previously mentioned compounds, the emergence of the topological states is unknown when described from the more fundamental perspective of quantum mechanically fluctuating individual mobile electrons, including electron-electron interaction.

To fully understand how the topological state in $\mathcal{S} = 1$ chains emerges from a fermionic description, one has to focus on the effects of electron interaction within the multi-orbital systems in which Hubbard and Hund's couplings are crucial ingredients. Here, we demonstrate that these couplings are sufficient for the onset of the topologically nontrivial phase. Specifically, upon increasing the strength of the Coulomb repulsion, we identify a previously unknown transition between topologically trivial and nontrivial ground-states. Our analysis unveils the threshold value of the interaction U_c where the Haldane gap opens. Although at U_c we also identify the emergence of zero-energy edge states and finite string order correlations (the signature properties of $\mathcal{S} = 1$ Haldane phase), surprisingly, the magnetic moments are far from being fully developed, and spin excitations still resemble those in the regime of weak $U \rightarrow 0$. Consequently, we here report that the Haldane phase is not limited by having $\mathcal{S} = 1$ moments. Specifically, its generalized existence can extend to unexpectedly small values of the interaction $U \sim W$, with W being the kinetic energy half-bandwidth.

Results

From two-orbital to Heisenberg model. We employ the zero-temperature density-matrix renormalization group method [4, 22, 23] (DMRG) to solve the 1D two-orbital Hubbard model (2oH) at half electronic filling ($n = 2$, i.e., two particles per site; one particle per orbital) and zero total magnetization $S_{\text{tot}}^z = 0$, relevant for Ni^{+2} -based compounds. The 2oH is given by

$$\begin{aligned}
 H_H = & \sum_{\gamma\gamma'\ell\sigma} t_{\gamma\gamma'} \left(c_{\gamma\ell\sigma}^\dagger c_{\gamma'\ell+1\sigma} + \text{H.c.} \right) + U \sum_{\gamma\ell} n_{\gamma\ell\uparrow} n_{\gamma\ell\downarrow} \\
 & + U' \sum_{\ell} n_{0\ell} n_{1\ell} - 2J_H \sum_{\ell} \mathbf{S}_{0\ell} \cdot \mathbf{S}_{1\ell} \\
 & + J_H \sum_{\ell} \left(P_{0\ell}^\dagger P_{1\ell} + \text{H.c.} \right). \quad (1)
 \end{aligned}$$

Here: $\ell = 1, \dots, L$ represents the site index, $\gamma = 0, 1$ the orbital index, and $\sigma = \uparrow, \downarrow$ the spin index. This model is generic and it can be derived from matrix elements of the fundamental $1/r$ Coulomb repulsion in the basis of atomic orbitals, following the Kanamori procedure [24]. Although challenging, the above model contains the most generic many-body interactions found in multiorbital systems: U and $U' = U - 5J_H/2$ represent the intra- and inter-orbital electron-electron Coulomb repulsion, respectively, while J_H accounts for the Hund rule, i.e., ferromagnetic exchange between spins at different orbitals; finally, $P_{0\ell}^\dagger P_{1\ell}$ with $P_{\gamma\ell}^\dagger = c_{\gamma\ell\uparrow}^\dagger c_{\gamma\ell\downarrow}^\dagger$ represents the doublon-holon exchange. We will focus on degenerate bands with $t_{00} = t_{11} = t = 0.5$ [eV], $t_{01} = t_{10} = 0$, and in the following, we will use the half-bandwidth of kinetic energy

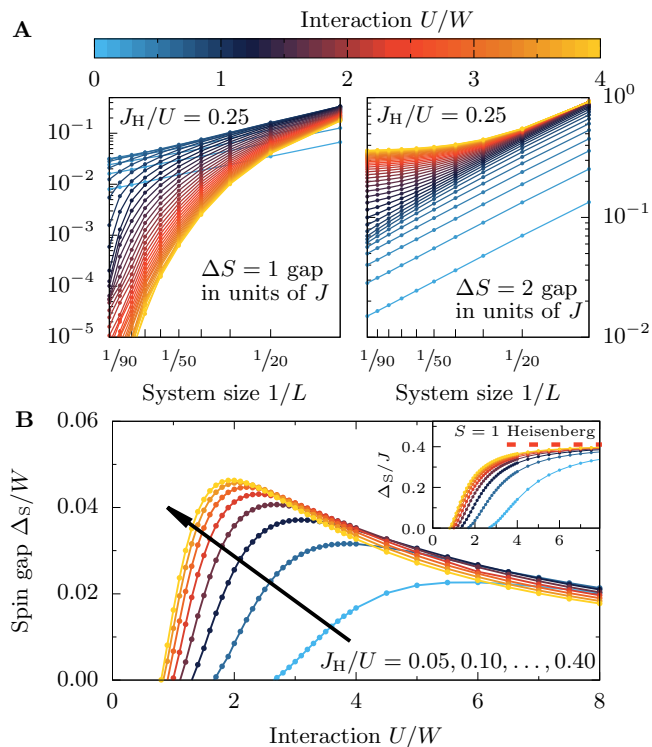


Figure 2. **Spin gaps.** **A** Finite-size scaling of $\Delta S = 1$ (left panel) and $\Delta S = 2$ (right panel) spin excitations for $J_H/U = 0.25$ and $L \in \{10, 20, \dots, 100\}$. Line color-code represents the value of the interaction U . Top to bottom: $J_H/U = 0.05, 0.10, \dots, 0.40$. Inset depicts the same data but renormalized by the effective spin exchange J . The saturation to the Haldane gap $\Delta_S/J \simeq 0.41$ is clearly visible (red dashed line).

as a unit, i.e., $W = 2t = 1[\text{eV}]$. While we will mostly consider the $J_H/U = 0.25$ case, other values of the Hund exchange will also be investigated (see Supplementary Note 1). Note that the $\mathbf{S}_{\gamma\ell}$ operators represent the spin-1/2 of electrons and that the above model preserves the $SU(2)$ symmetry provided that $U' = U - 5J_H/2$ and the doublon-holon exchange term is included [25].

The standard probe of spin excitations is the momentum q and energy ω resolved dynamical spin structure factor $S(q, \omega)$, which is the Fourier transform of the non-local Green's functions $\langle\langle \mathbf{T}_\ell \mathbf{T}_{\ell'} \rangle\rangle_\omega$ (see Methods), with \mathbf{T}_ℓ as the total on-site spin $\mathbf{T}_\ell = \sum_\gamma \mathbf{S}_{\gamma\ell}$. The calculated $S(q, \omega)$ is routinely compared to inelastic neutron scattering (INS) or resonant inelastic X-ray scattering data, also in the case of $S = 1$ compounds. With increasing strength of interaction U , the 2oH spectrum (Fig. 1A) develops from a continuum of $S = 1/2$ -like excitations at $U = 0$ [26, 27] to the well-established magnon-like excitations [28, 29] of the $S = 1$ Heisenberg model at large $U \gg W$. Renormalizing the frequency by the effective spin exchange, $J = 2t^2/(U + J_H)$ [20], yields qualitative agreement between the models at

$U/W \simeq 4$. As expected, for such value of interaction U , the average total magnetic moment is almost maximized $\mathbf{T}^2 = \mathcal{S}(\mathcal{S} + 1) \simeq 2$ and the charge fluctuations $\delta n = \langle n^2 \rangle - \langle n \rangle^2$ are vanishing (Fig. 1B).

The artificial broadening needed in the dynamical-DMRG method [30, 31], which physically mimics the influence of disorder, finite temperature, and measurements-device resolution, prevents us from extracting accurate values of the magnon gap directly from the spectrum of $S(q, \omega)$. Instead, the gaps can be obtained from the difference in ground-state energies of two magnetization sectors with different S_{tot}^z (with ΔS being the magnetization difference) at fixed electron density n . It is important to note that when working on a finite-size lattice, the $\Delta S = 1$ excitations of 2oH are always gapless when extrapolated to the thermodynamic limit $L \rightarrow \infty$ (Fig. 2A). For $U \rightarrow 0$, the gapless spin excitations manifest the physics of noninteracting fermions, with an inverse-linear dependence on the system size $\mathcal{O}(1/L)$ of the gap according to Lieb-Schultz-Mattis theorem [32]. In the opposite limit of the $S = 1$ Heisenberg model at $U \gg W$, the gapless $\Delta S = 1$ excitation originates in a four-fold degenerate ground-state (two-fold in the $S_{\text{tot}}^z = 0$ sector) with two $S = 1/2$ edge states [29, 33]. For a finite L , these edge states are split due to their overlap [34], which decays exponentially with increasing system size. See large- U data in Fig. 2A. Thus, within the open boundary condition system with edge states, the true magnon gap Δ_S can be extracted from $\Delta S = 2$ excitations [4, 35, 36]. Still, for $U \rightarrow 0$, the magnons are gapless with $\mathcal{O}(1/L)$ size dependence of the gap.

On the other hand, increasing the strength of U changes the nature of the scaling. At large U , we observe a saturation to a finite value in the $L \rightarrow \infty$ limit. This saturation is to the well-known Haldane gap $\Delta_S/J \simeq 0.41$ for $U \gtrsim 4$, confirming the accuracy of our procedure. Crucially, the finite-size scaling varying U reveals a novel critical (Hund J_H dependent, see Supplementary Note 1) value of the interaction $U_c = U_c(J_H)$ where the gap opens (Fig. 2B). For example, for $J_H/U = 0.25$ the magnons become gapped at $U_c/W \simeq 0.9$.

A remarkable result of our computational investigations is that the magnon gap Δ_S opens at a value of the interaction $U = U_c$ for which the overall spin excitations are *far* from the $S = 1$ Heisenberg model magnon-like spectrum. In fact, for $U/W \sim 1$, the spin excitations still visually resemble the noninteracting continuum of $S = 1/2$ -like moments, though with redistributed spectral weights (Fig. 1A).

Zero-energy edge modes. As mentioned, the exponential in the system size dependence of the $\Delta S = 1$ gaps (Fig. 2A) indicates the presence of edge states. To quantify them, we analyze (Fig. 3) the zero-frequency $\omega = 0$ dynamical spin-spin correlation functions between the edge and the bulk of the system, i.e., the non-local Green's functions $(-1)^\ell \langle\langle T_1^z T_\ell^z \rangle\rangle_{\omega=0}$, capable of capturing zero-energy modes. Here, the $(-1)^\ell$ prefactor removes the AFM staggered pattern. At small U ,

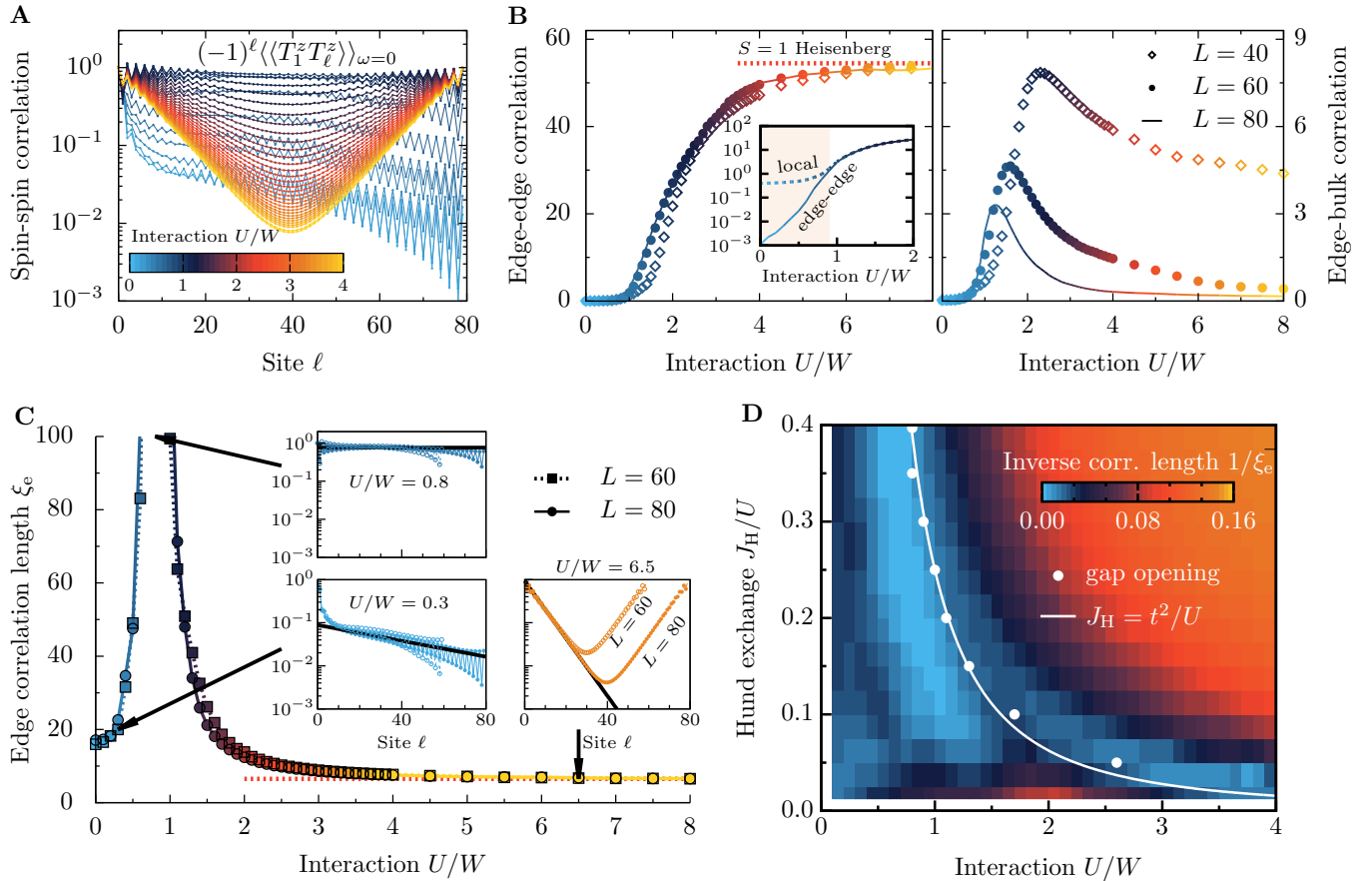


Figure 3. **Edge spin correlations.** **A** Distance ℓ dependence of the zero frequency $\omega = 0$ dynamical spin-spin correlations $(-1)^\ell \langle \langle T_1^z T_\ell^z \rangle \rangle_{\omega=0}$ for various values of interaction U (denoted by color-code). The results are normalized by the $\ell = 1$ value of the correlation function. **B** Edge-edge $|\langle \langle T_1^z T_\ell^z \rangle \rangle_{\omega=0}|$ (left panel) and edge-bulk $|\langle \langle T_1^z T_{L/2}^z \rangle \rangle_{\omega=0}|$ (right panel) dynamical spin correlations vs. interaction strength U . At U_c , we observe the appearance of finite edge-edge correlations, saturating at $U \gg W$ to the value given by the $S = 1$ Heisenberg model (red dashed line). **C** Extracted, Eq. (2), edge correlation length ξ_e vs. interaction strength U . Insets depict examples of spin-spin correlations for two system sizes ($L = 60$ and $L = 80$, together with fitted exponentials $\propto \exp(-\ell/\xi_e)$). All data are calculated at $J_H/U = 0.25$. **D** Interaction U/W - Hund exchange J_H/U phase diagram on the basis of inverse edge correlation length $1/\xi_e$ for $L = 60$. White points depict U_c obtained from the spin gap Δ_S opening, while the white line represents $J_H = t^2/U$.

the spin correlations decay exponentially with distance ℓ (Fig. 3A), as expected for a paramagnetic region. Increasing U leads to a slower decay, although still exponential. At $U \simeq U_c$, the $\omega = 0$ correlations are approximately site-independent. Note that this does not originate in any long-range order because the value of spin correlations decays with the system size (see Fig. 3B and the discussion below).

Interestingly, a characteristic V-shape of correlations develops above U_c . This is the manifestation of the edge states present at the (open) boundaries of the system [5]. In the $S = 1$ Heisenberg model, the zero-energy modes are not localized at a single edge site but decay exponentially with the correlation length $\xi_S \simeq 6.1$. This leads to finite (exponentially suppressed) AFM spin correlations up to half $\ell \sim L/2$ of the system. The increase of $\langle \langle T_1^z T_\ell^z \rangle \rangle_{\omega=0}$ for $\ell > L/2$ is exactly a consequence of cor-

related edge states: the edge-edge correlations are finite, while the edge-bulk correlations are vanishing.

To assess the development of spin-spin correlations in the 2oH system, especially the correlated edge states, we monitor the behaviour of the edge-edge and edge-bulk (Fig. 3B) values vs. the interaction U . The edge-edge correlations acquires a nonzero value at U_c (see Supplementary Note 2) and displays small finite-size effects. On the other hand, the finite value of the edge-bulk correlations decreases with system size L and vanishes in the $L \rightarrow \infty$ limit.

Furthermore, we can extract the interaction dependence of the edge correlation length (Fig. 3C) by fitting $\ell < L/2$ data of the 2oH to

$$(-1)^\ell \langle \langle T_1^z T_\ell^z \rangle \rangle_{\omega=0} \propto \exp(-\ell/\xi_e). \quad (2)$$

For $U/W > 4$ we reproduce $\xi_e \simeq \xi_S \simeq 6.1$, consistent

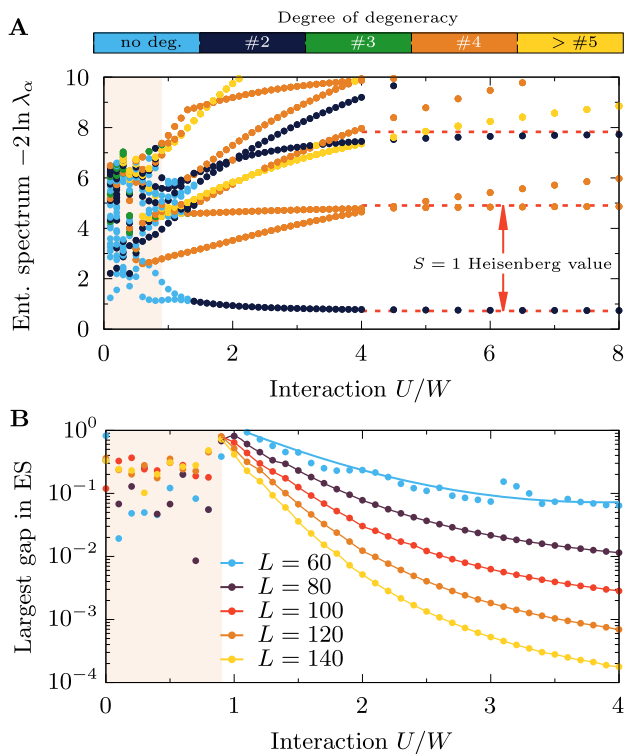


Figure 4. **Topological phase transition.** **A** Interaction U dependence of the entanglement spectrum $-2 \ln \lambda_\alpha$, obtained at $J_H/U = 0.25$ using a $L = 140$ site system partitioned in half. Color code depicts the number of occurrences of a given eigenvalue (number of degeneracies). The values for the $S = 1$ Heisenberg model are also displayed (red dashed lines). **B** Analysis of the largest gap in the entanglement spectrum for various system sizes $L = 60, 80, 100, 120, 140$ (see also Supplementary Note 3).

with dynamical spin structure factor $S(q, \omega)$ investigations of the $S = 1$ Heisenberg model physics. Interestingly, the extracted ξ diverges at U_c . This divergence reflects the site-independent correlations in this region (see Supplementary Note 2).

Topological phase transition. The opening at U_c of a spin gap Δ_S , the emergence of edge-edge correlations $\langle\langle T_1^z T_L^z \rangle\rangle_{\omega=0}$, and the diverging edge correlation length ξ_e all consistently indicate the existence of an interaction-induced topological phase transition between topologically trivial and nontrivial regions, with the emergence of the Haldane edge states at U_c . The topological phases can be identified by investigating the entanglement spectrum of the system [37, 38], i.e., the Schmidt coefficients λ_α of left/right ($|L\rangle/|R\rangle$) decomposed ground-state $|\text{gs}\rangle = \sum_\alpha \lambda_\alpha |L\rangle_\alpha |R\rangle_\alpha$, with λ_α^2 being the eigenvalues of the reduced density matrix of the partition. In the topologically nontrivial region, all λ_α 's are evenly degenerate. Consequently, the entanglement entropy $S_{vN} = -\sum_\alpha \lambda_\alpha^2 \ln \lambda_\alpha^2$ cannot drop below the $\ln 2$ value for any cut of the system, consistent with the presence of entangled $S = 1/2$ edge states. The analysis

of the 2oH model indicates that this condition is fulfilled for $U \gtrsim U_c$ (Fig. 4A). Detailed investigation of the largest gap (see Supplementary Note 3) in the entanglement spectrum (Fig. 4B) shows that the trivial region $U < U_c$ does not have any apparent structure in the λ_α eigenvalues. On the other hand, the largest gap decays exponentially with system size for any $U > U_c$ (though, with slower decay in the proximity of U_c) and vanishes in the thermodynamic limit $L \rightarrow \infty$.

In the context of the $S = 1$ Heisenberg model, the topological Haldane phase can also be detected by studying the non-local string order parameter [33, 39, 40]

$$\mathcal{O}_s(\ell) = - \left\langle A_m \exp \left(i\theta \sum_{n=m+1}^{m+\ell-1} A_n \right) A_{m+\ell} \right\rangle, \quad (3)$$

which for $\theta = \pi$ and $A_\ell = S_\ell^z$ measures the breaking of the discrete $Z_2 \times Z_2$ hidden symmetry (i.e., the dihedral group of π rotations). It is important to note that the phase $\theta = \pi$ was obtained via the valence bond state structure of the AKLT state. For a generic spin- S Heisenberg model, the string order phase becomes spin-dependent $\theta = \theta(S)$, i.e., it has to reflect the properties of a given VBS ground-state [41–44].

In the case of the 2oH model, for $U > U_c$, the π -string order \mathcal{O}_s does not decay (Fig. 5), as expected in the $S = 1$ Haldane phase. However, it is important to note that the total spin operator of 2oH, $A_\ell = T_\ell^z$, involves not only $S = 1$ but also $S = 1/2$ degrees of freedom and that for $U \simeq U_c$ the magnetic moment deviates strongly from $S = 1$ (Fig. 1B). Nevertheless, we observe a *finite* string order all the way down to $U = U_c \sim W$, showing that this type of order can exist in a fermionic system as well, even without well-defined moments. Interestingly, consistent with the topological phase transition at U_c , for $U < U_c$ the string order vanishes, and the system size dependence changes from weakly increasing with L (for $U > U_c$) to weakly decreasing with L (for $U < U_c$). The latter is consistent with the slow scaling of \mathcal{O}_s for $S = 1/2$ moments [45].

Discussion. The non-local character of the topological states allows for phase transitions even in 1D (rare phenomena due to the Mermin-Wagner theorem). Our numerical results indicate that the correlated one-dimensional two-orbital Hubbard model has a sharp transition at $U_c \sim W$ between a topologically trivial region and a generalized fermionic Haldane phase with edge states. Surprisingly, the magnetic moments are not yet fully developed in a vast region of the topological phase (Fig. 1B), and thus the $S = 1$ Heisenberg model-like description cannot be applied directly, and it is not necessary to describe the physics of the fermionic generalized Haldane phase presented here. Actually, our analysis shows that the gapped ground-state with finite string order survives down to $U \sim W \sim \mathcal{O}(t)$. Consequently, this result indicates that a VBS-like state, similar to the AKLT state, could be formulated [46] even with mobile fermions. It seems true despite the fact that the length

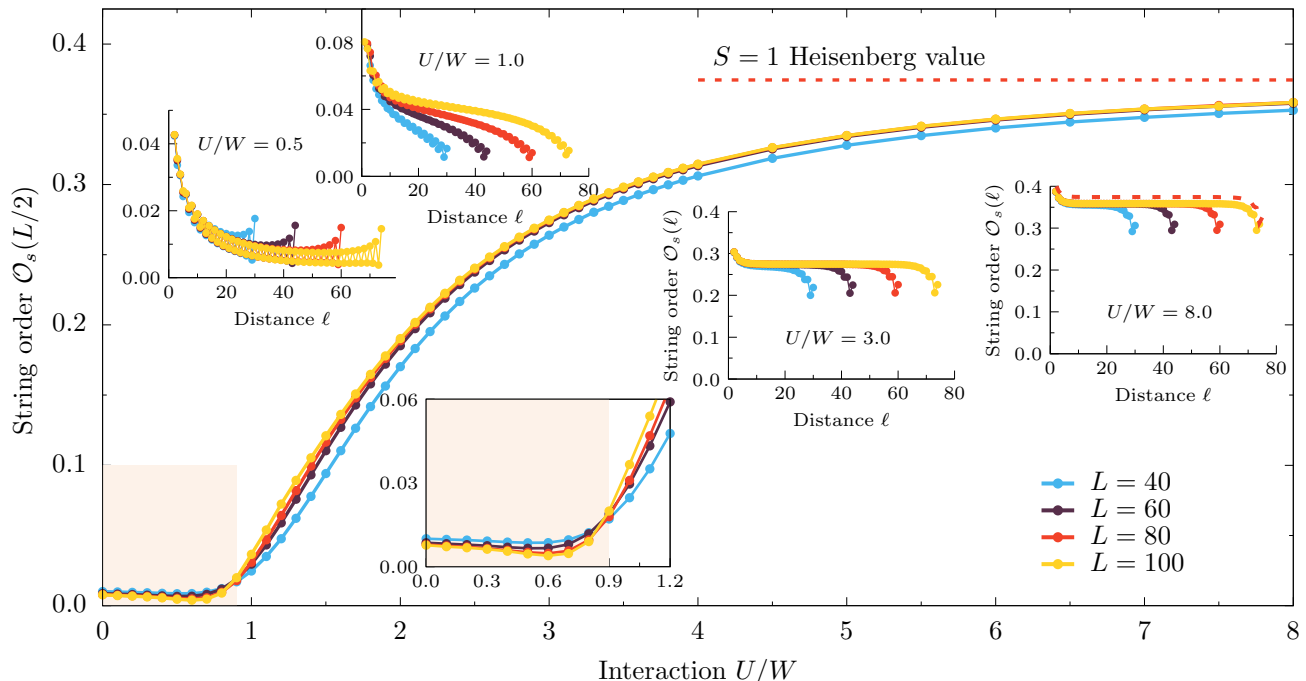


Figure 5. **String order.** Interaction U dependence of the string order parameter $\mathcal{O}_s(\ell)$ with $\theta = \pi$ phase at $\ell = L/2$ distance in the bulk ($m = L/4$). Upper insets depicts $\mathcal{O}_c(\ell)$ vs. distance ℓ for $U = 0.5, 1.0, 3.0, 8.0$ (left to right). The lower inset depicts a zoom to the proximity of the phase transition U_c , with the shaded region depicting the trivial phase. All data are evaluated at $J_H/U = 0.25$ using $L = 40, 60, 80, L = 100$ site systems.

scale of spin-spin correlations indicates the spatially extended character of the ground-state, although with moments small in value. Our detailed interaction U and Hund exchange J_H investigation (Fig. 3D) indicates that the $SU(2)$ symmetric system undergoes the transition at $J_H \simeq t^2/U$, and consequently a finite $U \sim W$ is necessary for the onset of the non-topological-topological phase transition in real materials.

Furthermore, our results indicate that the details of the band structure, i.e., of the hopping matrix $t_{\gamma\gamma'}$, are not crucial for our findings. Up to now, we have considered degenerate bands, i.e., $t_{00} = t_{11} = 0.5$ [eV] and $t_{01} = t_{10} = 0$. In Fig. 6 we present additional results of edge correlation length ξ_e (discussed in Fig. 3) and string order parameter $\mathcal{O}_s(L/2)$ (discussed in Fig. 5) for non-degenerate bands ($t_{00} = 0.5$ [eV], $t_{11} = 0.3$ [eV], $t_{01} = t_{10} = 0$, with $W = 1$ [eV]) and strongly hybridized orbitals ($t_{00} = 0.5$ [eV], $t_{11} = 0.3$ [eV], $t_{01} = t_{10} = 0.5$ [eV], with $W = 1.8$ [eV]). For all considered cases, we find the transition (identified by diverging ξ_e and the onset of non-zero \mathcal{O}_s) to the Haldane phase at a finite value of interaction U . Consequently, our results are relevant for various low-dimensional $S = 1$ compounds, irrespective of kinetic energy details, i.e., for recently investigated platforms such as the van der Waals oxide dichlorides MOX_2 ($M=V, Ta, Nb, Ru, Os$ and $X=\text{halogen element}$) [47] or metal-organic structures [48]. Another promising candidate to test the prediction of our work is the van

der Waals quasi-1D material $OsCl_4$ [49].

Also, one could expect that for $J_H \gg U$ (i.e., when the system always has well-developed on-site triplets formed by electrons), even small interaction will induce the Haldane phase. However, such region of parameter space is unrealistic because for $J_H/U > 0.4$ the inter-orbital interaction $U' = U - 5J_H/2$ becomes attractive $U' < 0$. It is therefore evident that setups with coupled $S = 1/2$ triplets represent, from the electron system perspective, broken spin rotation with $U' \neq U - 5J_H/2$. Previous analysis of the Haldane phase in such setups indicates its fragility with respect to charge fluctuations [16–18]. Our results indicate that within a two-orbital setup, the Haldane phase is robust down to rather small values of the interaction U , in a regime where the magnetic moments are barely developed. Thus, our results are generalizing the ideas of Haldane for $S = 1$ spin Heisenberg models into unexplored territory involving delocalized electrons. The structure of Haldane edge states was previously investigated, e.g., via INS experiments [10]. However, our results indicate that the energy gap separating the edge modes from the magnon-like excitations can be small (even exponentially small at the transition $U \sim U_c$, see Fig. 2B). Similarly, the intensity of such a modes is diminishing close the transition (see Fig. 3B). As a consequence, neutron scattering (as a global probe of the sample) would not necessarily be the best tool. An alternative would be local probes as, e.g., nuclear magnetic

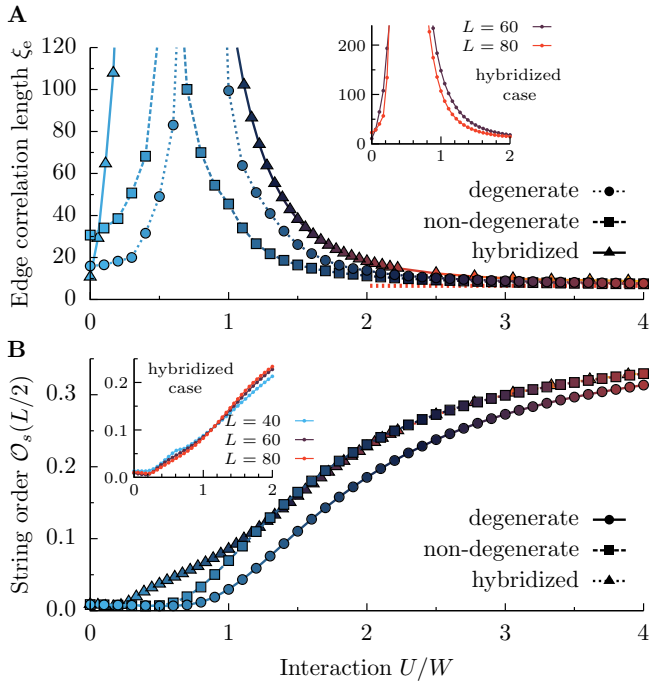


Figure 6. **Band structure dependence.** Interaction U/W dependence of **A** edge correlation length ξ_e and **B** string order parameter $\mathcal{O}_s(L/2)$ for degenerate, non-degenerate bands, and also for the strongly hybridized case (see text for details). Main panels depict $L = 60$ and $J_H/U = 0.25$ data, while insets depict finite-size scaling of strongly hybridized cases.

resonance experiments [50], exploiting the large edge correlation length $\xi_e \gg \xi_S$ (quantified by the decay of staggered magnetization at the edges of the system).

Methods

DMRG method. The Hamiltonians and observables discussed here were studied using the zero-temperature density matrix renormalization group (DMRG) method [4, 23] within the single center site approach [22], where the dynamical correlation functions are evaluated via the dynamical-DMRG [30, 31], i.e., calculating spectral functions directly in frequency space with the correction-vector method using the Krylov decomposition [31]. We have kept up to $M = 3072$ states, performed at least 15 sweeps, and used $A = 0.001$ vector-offset in the single-site DMRG approach, allowing to accurately simulate system sizes up to $L \lesssim 140$ sites of the two-orbital Hubbard model. Consequently, the error bars on the numerical results are smaller than the data points.

Dynamical spin structure factor. The dynamical spin structure factors are evaluated as

$$S(q, \omega) = \frac{2}{L+1} \sum_{\ell=1}^L \cos[(\ell - L/2)q] \langle \langle \mathbf{T}_\ell \mathbf{T}_{L/2} \rangle \rangle_\omega, \quad (4)$$

where $q = n\pi/(L+1)$, $n = 0, \dots, L$, and non-local

Green's function is given by

$$\langle \langle \mathbf{T}_m \mathbf{T}_n \rangle \rangle_\omega = -\frac{1}{\pi} \text{Im} \langle \text{gs} | \mathbf{T}_m \frac{1}{\omega + i\eta - H + \epsilon_0} \mathbf{T}_n | \text{gs} \rangle. \quad (5)$$

Here $|\text{gs}\rangle$ represents the ground-state with energy ϵ_0 . The $S(q, \omega)$ spectra presented in Fig. 1A of the main text were calculated with the frequency resolution $\delta\omega/J \simeq 0.03$ and broadening $\eta = 2\delta\omega$ [note the U -dependence of the spin exchange $J = 2t^2/(U + J_H)$].

Largest gap in the entanglement spectrum. In order to find the largest gap in the entanglement spectrum, first we have calculated consecutive gaps $\delta_n = \min(\ln \lambda_n - \ln \lambda_{n-1}; \ln \lambda_{n+1} - \ln \lambda_n)$. The largest gap is then obtained from $\max(\delta_1, \delta_2, \dots)$.

Data availability

The data generated in this study have been deposited in the Zenodo database under accession code <https://doi.org/10.5281/zenodo.7854617>.

Code availability

We have used the DMRG++ computer program developed at Oak Ridge National Laboratory. The code that supports this study is available at Oak Ridge National Laboratory repository https://code.ornl.gov/gonzalo_3/dmrgpp. The input scripts for the DMRG++ package to reproduce our results can be found at <https://bitbucket.org/herbrychjacek/corrwro/> and on the DMRG++ webpage.

Acknowledgments M.M. acknowledges support from the National Science Centre (NCN), Poland, via project 2020/37/B/ST3/00020. M.Ś. and J.H. acknowledge grant support from the National Science Centre (NCN), Poland, via project 2019/35/B/ST3/01207. A.N. acknowledges support from the Max Planck-UBC-UTokyo Center for Quantum Materials and Canada First Research Excellence Fund (CFREF) Quantum Materials and Future Technologies Program of the Stewart Blusson Quantum Matter Institute (SBQMI), and the Natural Sciences and Engineering Research Council of Canada (NSERC). G.A. was partly supported by the Scientific Discovery through Advanced Computing (SciDAC) program funded by the U.S. DOE, Office of Science, Advanced Scientific Computing Research and BES, Division of Materials Sciences and Engineering. E.D. was supported by the US Department of Energy, Office of Science, Basic Energy Sciences, Materials Sciences and Engineering Division. Part of the calculations have been carried out using resources provided by Wroclaw Centre for Networking and Supercomputing.

Author contributions J.H. conceived the study. A.J., M.M., E.D., and J.H. planned the project. A.J., M.Ś., and J.H. performed the numerical experiments and analyzed the data. A.N. and G.A. developed and tested the simulation codes. M.M., E.D., and J.H. wrote the manuscript. All authors provided comments on the pub-

lication.

Competing interests The authors declare no com-

peting interests.

-
- [1] F. D. M. Haldane, “Nonlinear Field Theory of Large-Spin Heisenberg Antiferromagnets: Semiclassically Quantized Solitons of the One-Dimensional Easy-Axis Néel State,” *Phys. Rev. Lett.* **50**, 1153 (1983).
- [2] F. D. M. Haldane, “Continuum dynamics of the 1-D Heisenberg antiferromagnet: Identification with the O(3) nonlinear sigma model,” *Phys. Lett. A* **93**, 464 (1983).
- [3] I. Affleck, T. Kennedy, E. H. Lieb, and H. Tasaki, “Rigorous results on valence-bond ground states in antiferromagnets,” *Phys. Rev. Lett.* **59**, 799 (1987).
- [4] S. R. White, “Density matrix formulation for quantum renormalization groups,” *Phys. Rev. Lett.* **69**, 2863 (1992).
- [5] S. R. White and D. A. Huse, “Numerical renormalization-group study of low-lying eigenstates of the antiferromagnetic $S = 1$ Heisenberg chain,” *Phys. Rev. B* **48**, 3844 (1993).
- [6] T. Jolicoeur and O. Golinelli, “Physics of integer-spin antiferromagnetic chains: Haldane gaps and edge states,” *C. R. Chimie* **22**, 445 (2019).
- [7] E. H. Kim, G. Fáth, J. Sólyom, and D. J. Scalapino, “Phase transitions between topologically distinct gapped phases in isotropic spin ladders,” *Phys. Rev. B* **62**, 14965 (2000).
- [8] I. A. Zaliznyak, S.-H. Lee, and S. V. Petrov, “Continuum in the Spin-Excitation Spectrum of a Haldane Chain Observed by Neutron Scattering in CsNiCl_3 ,” *Phys. Rev. Lett.* **87**, 017202 (2001).
- [9] M. Kenzelmann, R. A. Cowley, W. J. L. Buyers, Z. Tun, R. Coldea, and M. Enderle, “Properties of Haldane excitations and multiparticle states in the antiferromagnetic spin-1 chain compound CsNiCl_3 ,” *Phys. Rev. B* **66**, 024407 (2002).
- [10] M. Kenzelmann, G. Xu, I. A. Zaliznyak, C. Broholm, J. F. DiTusa, G. Aeppli, T. Ito, K. Oka, and H. Takagi, “Structure of End States for a Haldane Spin Chain,” *Phys. Rev. Lett.* **90**, 087202 (2003).
- [11] P. Sompert, S. Hirthe, D. Bourgund, T. Chalopin, J. Bibo, J. Koepsell, P. Bojović, R. Verresen, F. Pollmann, G. Salomon, C. Gross, T. A. Hilker, and I. Bloch, “Realizing the symmetry-protected Haldane phase in Fermi–Hubbard ladders,” *Nature* **606**, 484 (2022).
- [12] A. Nag, A. Nocera, S. Agrestini, M. Garcia-Fernandez, C. Walters, S.-W. Cheong, S. Johnston, and K.-J. Zhou, “Quadrupolar magnetic excitations in an isotropic spin-1 antiferromagnet,” *Nat. Commun.* **13**, 2327 (2022).
- [13] P. Jelínek, “Quantum spin chains go organic,” *Nat. Chem.* **15**, 12 (2023).
- [14] E. G. Dalla Torre, E. Berg, and E. Altman, “Hidden order in 1d bose insulators,” *Phys. Rev. Lett.* **97**, 260401 (2006).
- [15] E. Berg, E. G. Dalla Torre, T. Giamarchi, and E. Altman, “Rise and fall of hidden string order of lattice bosons,” *Phys. Rev. B* **77**, 245119 (2008).
- [16] F. Anfuso and A. Rosch, “Fragility of string orders,” *Phys. Rev. B* **76**, 085124 (2007).
- [17] F. Anfuso and A. Rosch, “String order and adiabatic continuity of haldane chains and band insulators,” *Phys. Rev. B* **75**, 144420 (2007).
- [18] S. Moudgalya and F. Pollmann, “Fragility of symmetry-protected topological order on a Hubbard ladder,” *Phys. Rev. B* **91**, 155128 (2015).
- [19] O. V. Maximova, S. V. Streltsov, and A. N. Vasiliev, “Long range ordered, dimerized, large-D and Haldane phases in spin 1 chain compounds,” *Crit. Rev. Solid State Mater. Sci.* **46**, 371 (2021).
- [20] H. Onishi and T. Hotta, “Orbital-controlled magnetic transition between gapful and gapless phases in the Haldane system with t_{2g} -orbital degeneracy,” *Phys. Rev. B* **70**, 100402 (2004).
- [21] L. de’ Medici, J. Mravlje, and A. Georges, “Janus-Faced Influence of Hund’s Rule Coupling in Strongly Correlated Materials,” *Phys. Rev. Lett.* **107**, 256401 (2011).
- [22] S. R. White, “Density matrix renormalization group algorithms with a single center site,” *Phys. Rev. B* **72**, 180403 (2005).
- [23] U. Schollwöck, “The density-matrix renormalization group,” *Rev. Mod. Phys.* **77**, 259 (2005).
- [24] E. Dagotto, T. Hotta, and A. Moreo, “Colossal magnetoresistant materials: the key role of phase separation,” *Phys. Rep.* **344**, 1 (2001).
- [25] A. Georges, L. de’ Medici, and J. Mravlje, “Strong Correlations from Hund’s Coupling,” *Annu. Rev. Condens. Matter Phys.* **4**, 137 (2013).
- [26] G. Muller, H. Thomas, M. W. Puga, and H. Beck, “Quantum spin dynamics of the one-dimensional planar antiferromagnet,” *J. Phys. C: Solid State Phys* **14**, 3399 (1981).
- [27] P. Laurell, A. Scheie, D. A. Tennant, S. Okamoto, G. Alvarez, and E. Dagotto, “Magnetic excitations, nonclassicality, and quantum wake spin dynamics in the Hubbard chain,” *Phys. Rev. B* **106**, 085110 (2022).
- [28] S. R. White and I. Affleck, “Spectral function for the $S = 1$ Heisenberg antiferromagnetic chain,” *Phys. Rev. B* **77**, 134437 (2008).
- [29] J. Becker, T. Köhler, A. C. Tiegel, S. R. Manmana, S. Wessel, and A. Honecker, “Finite-temperature dynamics and thermal intraband magnon scattering in Haldane spin-one chains,” *Phys. Rev. B* **96**, 060403 (2017).
- [30] E. Jeckelmann, “Dynamical density-matrix renormalization-group method,” *Phys. Rev. B* **66**, 045114 (2002).
- [31] A. Nocera and G. Alvarez, “Spectral functions with the density matrix renormalization group: Krylov-space approach for correction vectors,” *Phys. Rev. E* **94**, 053308 (2016).
- [32] I. Affleck and E. H. Lieb, “A proof of part of Haldane’s conjecture on spin chains,” *Lett. Math. Phys.* **12**, 57 (1986).
- [33] T. Kennedy and H. Tasaki, “Hidden symmetry breaking and the Haldane phase in $S = 1$ quantum spin chains,” *Phys. Rev. B* **147**, 431 (1992).
- [34] J. Fraxanet, D. González-Cuadra, T. Pfau, M. Lewenstein, T. Langen, and L. Barbiero, “Topological Quantum Critical Points in the Extended Bose-Hubbard

- Model,” *Phys. Rev. Lett.* **128**, 043402 (2022).
- [35] S. Qin, T.-K. Ng, and Z.-B. Su, “Edge states in open antiferromagnetic Heisenberg chains,” *Phys. Rev. B* **52**, 12844 (1995).
- [36] S. Yamamoto and S. Miyashita, “Low-lying excitations in the $S = 1$ antiferromagnetic Heisenberg chain,” *Phys. Lett. A* **235**, 545 (1997).
- [37] H. Li and F. D. M. Haldane, “Entanglement Spectrum as a Generalization of Entanglement Entropy: Identification of Topological Order in Non-Abelian Fractional Quantum Hall Effect States,” *Phys. Rev. Lett.* **101**, 010504 (2008).
- [38] F. Pollmann, A. M. Turner, E. Berg, and M. Oshikawa, “Entanglement spectrum of a topological phase in one dimension,” *Phys. Rev. B* **81**, 064439 (2010).
- [39] M. den Nijs and K. Rommelse, “Preroughening transitions in crystal surfaces and valence-bond phases in quantum spin chains,” *Phys. Rev. B* **40**, 4709 (1989).
- [40] T. Kennedy and H. Tasaki, “Hidden $Z_2 \times Z_2$ symmetry breaking in Haldane-gap antiferromagnets,” *Phys. Rev. B* **45**, 304 (1992).
- [41] M. Oshikawa, “Hidden $Z_2 \times Z_2$ symmetry in quantum spin chains with arbitrary integer spin,” *J. Phys.: Condens. Matter* **4**, 7469 (1992).
- [42] K. Totsuka and M. Suzuki, “Matrix formalism for the VBS-type models and hidden order,” *J. Phys.: Condens. Matter* **7**, 1639 (1995).
- [43] S. Qin, J. Lou, L. Sun, and C. Chen, “Nonlocal Topological Order in Antiferromagnetic Heisenberg Chains,” *Phys. Rev. Lett.* **90**, 067202 (2003).
- [44] F. Pollmann, E. Berg, A. M. Turner, and M. Oshikawa, “Symmetry protection of topological phases in one-dimensional quantum spin systems,” *Phys. Rev. B* **85**, 075125 (2012).
- [45] J. Lou, S. Qin, and C. Chen, “String Order in Half-Integer-Spin Antiferromagnetic Heisenberg Chains,” *Phys. Rev. Lett.* **91**, 087204 (2003).
- [46] N. D. Patel, N. Kaushal, A. Nocera, G. Alvarez, and E. Dagotto, “Emergence of superconductivity in doped multiorbital Hubbard chains,” *npj Quantum Mater.* **5**, 27 (2020).
- [47] Y. Zhang, L.-F. Lin, A. Moreo, T. A. Maier, G. Alvarez, and E. Dagotto, “Strongly anisotropic electronic and magnetic structures in oxide dichlorides RuOCl_2 and OsOCl_2 ,” *Phys. Rev. B* **105**, 174410 (2022).
- [48] P. Tin, M. J. Jenkins, J. Xing, N. Caci, Z. Gai, R. Jin, S. Wessel, J. Krzystek, C. Li, L. L. Daemen, Y. Cheng, and Xue Z.-L., “Haldane topological spin-1 chains in a planar metal-organic framework,” *Nat. Commun.* **14**, 5454 (2023).
- [49] Y. Zhang, L.-F. Lin, A. Moreo, and E. Dagotto, “Electronic and magnetic properties of quasi-one-dimensional osmium halide OsCl_4 ,” *Applied Physics Letters* **120**, 023101 (2022).
- [50] J.-P. Renard, L.-P. Regnault, and M. Verdaguer, “Haldane quantum spin chains,” in *Magnetism: Molecules to Materials* (John Wiley & Sons, Ltd, 2004) Chap. 2, p. 49.

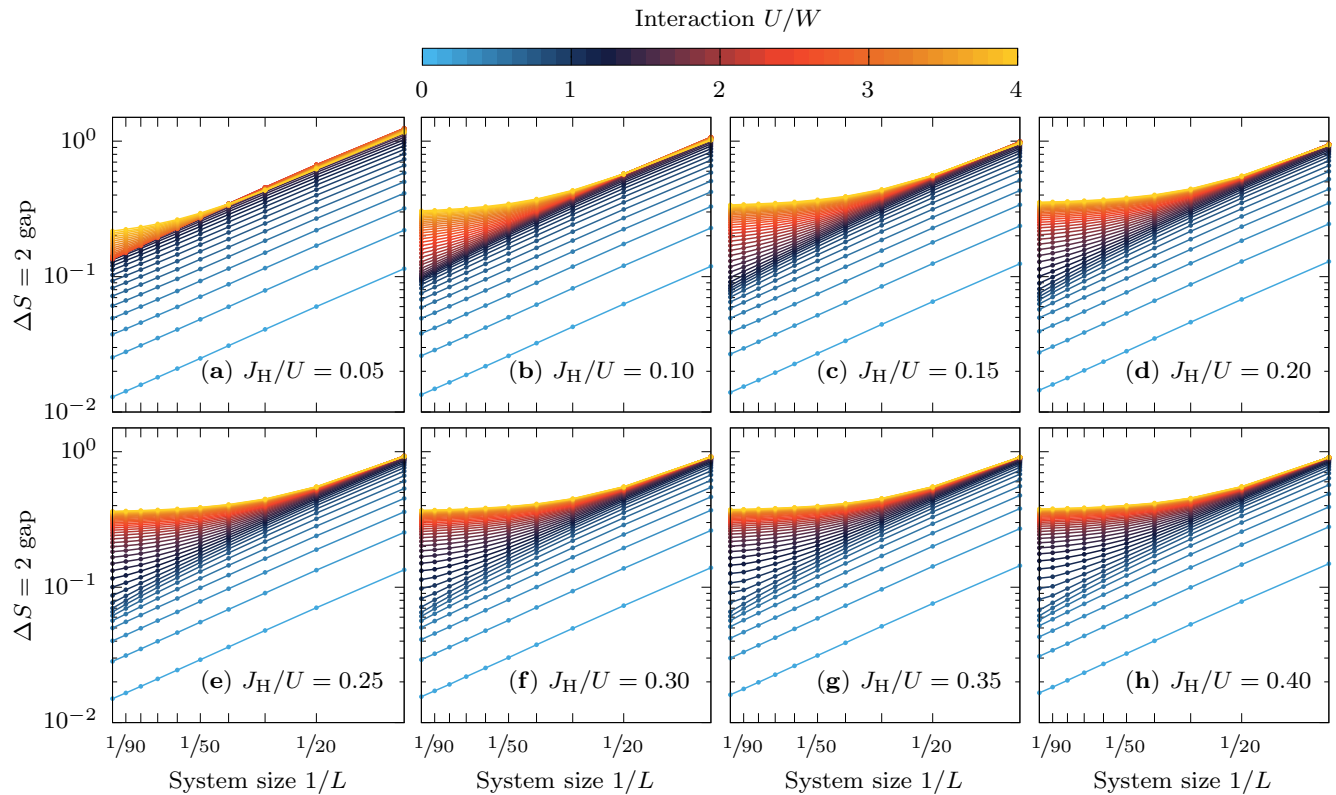
SUPPLEMENTARY INFORMATION

Transition to the Haldane phase driven by electron-electron correlations

by A. Jazdzewska, M. Mierzejewski, M. Środa, A. Nocera, G. Alvarez, E. Dagotto, and J. Herbrych

SUPPLEMENTARY NOTE 1: GAP ANALYSIS.

In Supplementary Fig. 1, we present the finite-size $1/L$ and interaction U dependence of the $\Delta S = 2$ gap (the magnon gap Δ_S/J) for various values of the Hund exchange $J_H/U = 0.05, 0.10, \dots, 0.40$. The main text displays the results of $1/L$ extrapolations of this data in Fig. 2B.

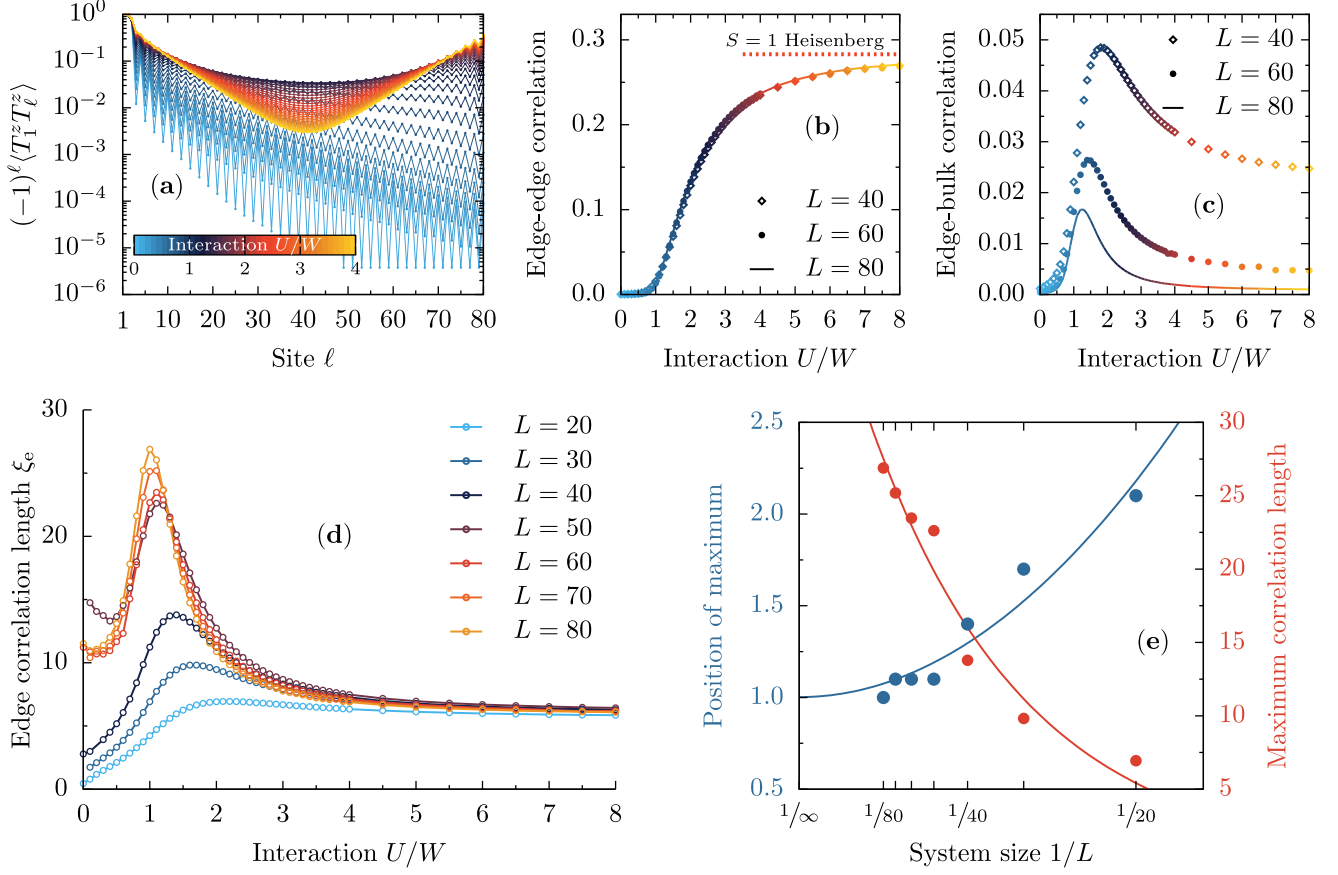


Supplementary Figure 1. **Spin gaps.** Finite-size scaling of $\Delta S = 2$ excitations (magnon gaps) for $J_H/U = 0.05, 0.10, \dots, 0.40$ and $L \in \{10, 20, \dots, 100\}$. Line color-code represents the value of interaction U . All data in units of spin exchange $J = 2t^2/(U + J_H)$. The saturation to the finite value (to the Haldane gap $\Delta_S/J \simeq 0.41$) is clearly visible in all panels.

SUPPLEMENTARY NOTE 2: STATIC AND DYNAMIC SPIN CORRELATIONS.

In the main text, we have described how the dynamical spin-spin correlation, i.e., the non-local Green's function $\langle\langle T_1^z T_\ell^z \rangle\rangle_{\omega=0}$, behave vs. distance ℓ and strength of the interaction U . Here, we present additional results for the static spin correlations, $\langle T_1^z T_\ell^z \rangle = \langle \text{gs} | T_1^z T_\ell^z | \text{gs} \rangle$.

In Supplementary Fig. 2, we present the analysis of the static $\langle T_1^z T_\ell^z \rangle$, similar to the one presented in Fig. 3 of the main text. As evident from panels (a-d), the overall behaviour of $\langle T_1^z T_\ell^z \rangle$ is almost identical to the zero-frequency $\omega = 0$ data. The main difference between the static and the dynamic correlation function can be observed in the extracted edge correlation length ξ_e close to the transition $U \sim U_c$ [compare Fig. 3C of the main text and Supplementary Fig. 2(d)]. I.e., the edge correlation length extracted from $\langle\langle T_1^z T_\ell^z \rangle\rangle_{\omega=0}$ data is much sharper than the



Supplementary Figure 2. **Static spin correlations.** (a) Distance ℓ dependence of static spin-spin correlations $(-1)^\ell \langle T_1^z T_\ell^z \rangle$ for various values of interaction U (denoted by color code). The results are normalized by the $\ell = 1$ value of the correlation function. (b) Edge-edge $|\langle T_1^z T_L^z \rangle|$ and (c) edge-bulk $|\langle T_1^z T_{L/2}^z \rangle|$ spin correlations vs. interaction strength U/W . At U_c , one observes the appearance of finite edge-edge correlations, saturating at $U \gg W$ to the value given by the $S = 1$ Heisenberg model (red dashed line). (d) Edge correlation length ξ_e vs. interaction U strength, extracted from $(-1)^\ell \langle T_1^z T_\ell^z \rangle = a \exp(-\ell/\xi_e)$ for $\ell < L/2$. (e) System-size dependence of the position of (blue points, left y-axis) and the value (red points, right y-axis) of the maximum edge correlation length. All data calculated for $J_H/U = 0.25$.

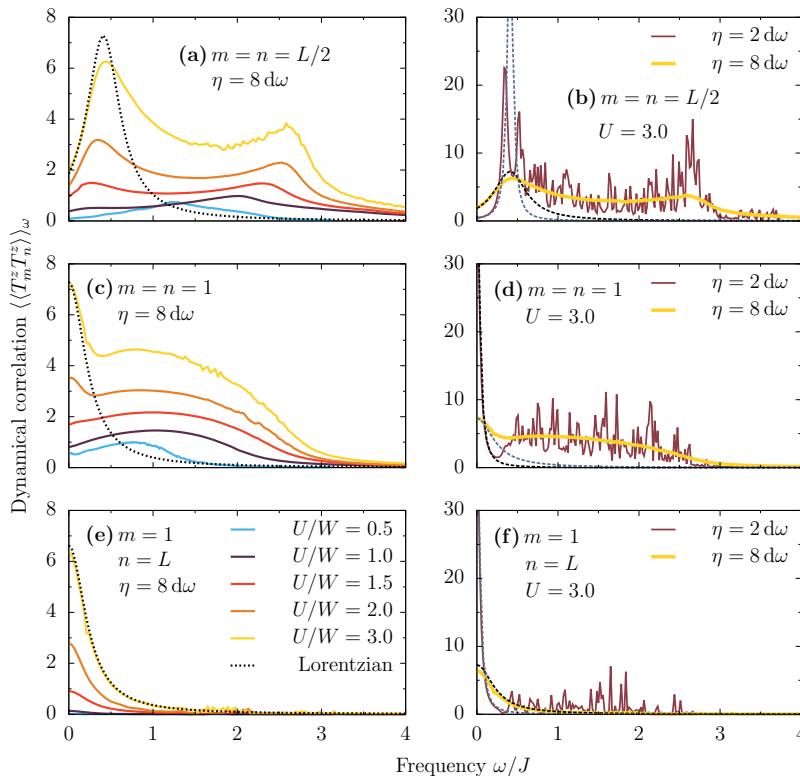
one extracted from the static $\langle T_1^z T_\ell^z \rangle$. Nevertheless, the scaling with the system size [see Supplementary Fig. 2(e)] of the position of the maximum of ξ_e as well as the value itself indicate a transition at U_c .

To understand the difference between static and dynamic results, consider the sum rule relating (at zero temperature) both of these quantities, i.e.,

$$\langle T_m^z T_n^z \rangle = \int_0^\infty d\omega \langle \langle T_m^z T_n^z \rangle \rangle_\omega. \quad (1)$$

It is evident that both approaches would yield the same behaviour if $\langle \langle T_m^z T_n^z \rangle \rangle_\omega = \delta(\omega)$. However, our analysis presented in Supplementary Fig. 3 indicates that the behaviour of the non-local Green's function $\langle \langle T_m^z T_n^z \rangle \rangle_\omega$ strongly depends on the pair of sites (m, n) considered. Note that, in the presented analysis, we have used finite broadening η [see Eq. (5)]. Consequently, all sharp features of the spectrum are broadened by a Lorentzian.

Within the fermionic Haldane phase, $U > U_c$, the spectrum of the bulk of the system, $m \sim n \sim L/2$, has only the incoherent part $\omega > 0$, and it is gapped; see Supplementary Fig. 3(a,b). Such behaviour is expected because (m, n) elements contribute (via the Fourier transform) to the overall dispersion relation presented in Fig. 1 of the main text. On the other hand, the correlation between the edge $m = 1$ and the rest of the system needs more attention: (i) consistent with the phenomenology of zero-energy edge modes, the edge-edge $(m, n) = (1, L)$ dynamical correlations contain only the $\omega = 0$ δ -function (broaden by the Lorentzian in our numerical investigation), see



Supplementary Figure 3. **Dynamical spin correlations** $\langle\langle T_m^z T_n^z \rangle\rangle_\omega$. Shown are the frequency ω dependence of the local Green's function in (a,b) the bulk of the system $m = n = L/2$ and in (b,c) at the edge $m = n = 1$. (d,e) The non-local Green function between edges of the system ($m = 1, n = L$). In all plots, color solid curves represent data for various values of interaction $U/W = 0.5, 1.0, \dots, 3.0$, $J_H/U = 0.25$, and $\eta = 8d\omega$ (left column) and $\eta = 2d\omega$ (right column). The dashed line represents the Lorentzian.

Supplementary Fig. 3(c,d). Consequently $\langle T_1^z T_\ell^z \rangle \simeq \langle\langle T_1^z T_\ell^z \rangle\rangle_{\omega=0}$. (ii) Edge-bulk correlation ($1, \sim L/2$) vanishes, again, consistent with the presence of the edge states (not shown). (iii) However, in the proximity of the edges (for $m \sim n \sim 1$), the dynamical correlations contain both coherent $\omega \sim 0$ (edge mode) and incoherent $\omega > 0$ parts [see Supplementary Fig. 3(e,f)], and $\langle T_1^z T_{m \sim 1}^z \rangle \neq \langle\langle T_1^z T_{m \sim 1}^z \rangle\rangle_{\omega=0}$.

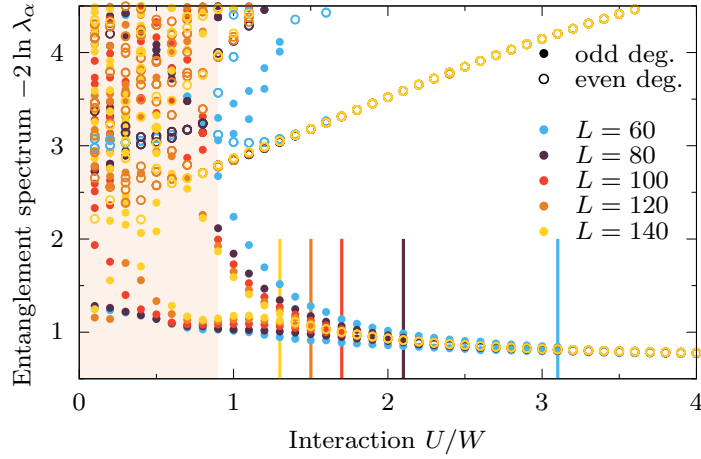
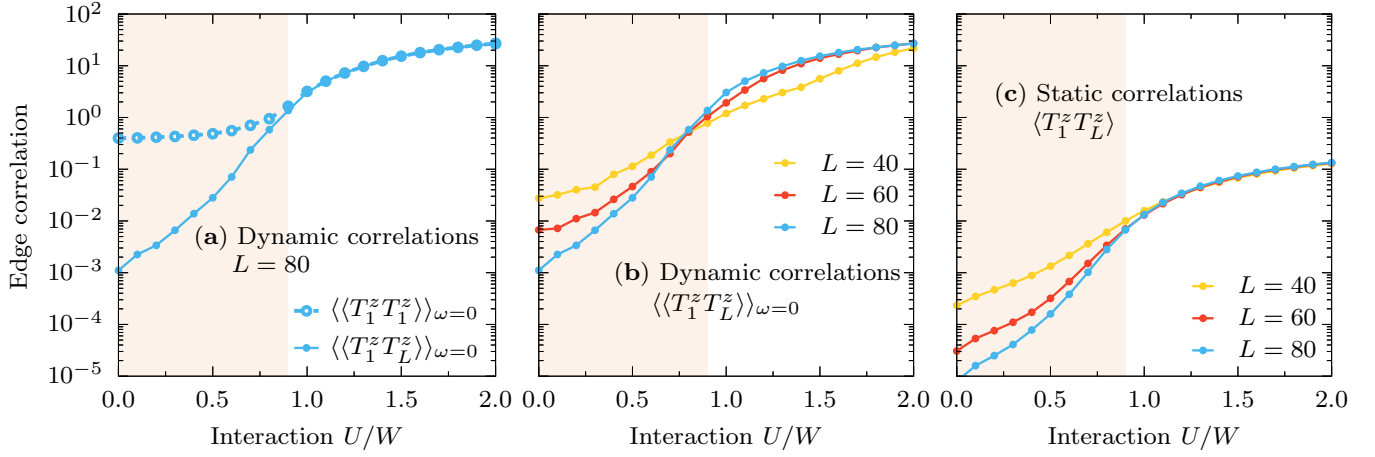
Finally, in Supplementary Fig. 4, we present additional evidence for the topological phase transition at $U = U_c \simeq 0.9W$ (for $J_H/U = 0.25$) from spin correlation data.

(1) In panel (a), we compare the local Green's function $n = m = 1$ and non-local edge-edge correlations $n = 1, m = L$ at zero-frequency $\omega = 0$. The change in the local value is related to the development of the magnetic moment \mathcal{S} . On the other hand, the non-local (edge-edge) probes only the appearance of edge zero-modes (as discussed in the main text). It is evident from the presented results that both quantities merge at $U = U_c$, consistent with the presence of the zero frequency edge modes for $U > U_c$.

(2) In panels (b) and (c), we present the same data as in Fig. 3B of the main text and Supplementary Fig. 2(b), respectively, in a log- y scale. Evidently, for $U > U_c$, the non-zero correlation functions do not originate from finite-size effects. On the other hand, for $U < U_c$, the values of edge-edge correlations (both static and dynamic) decay exponentially with system size.

SUPPLEMENTARY NOTE 3: ENTANGLEMENT SPECTRUM.

Supplementary Fig. 5 depicts additional results for the entanglement spectrum $-2 \ln \lambda_\alpha$. Consistent with the discussion presented in the main text, the value of the interaction U for which the spectrum is evenly degenerate moves to U_c with increasing system size L (see also Fig. 4 of the main text). Furthermore, it is evident from the presented results that the λ_α spectrum does not contain any apparent structure for $U < U_c$, and the condition [i.e., $\ln \lambda_{i+1} - \ln \lambda_i \leq 0.01$] of evenly degenerate entanglement spectrum is not fulfilled.



Supplementary Figure 5. **Entanglement entropy spectrum.** Interaction U/W dependence of the entanglement spectrum $-2 \ln \lambda_\alpha$, obtained for $J_H/U = 0.25$ and $L = 60, 80, \dots, 140$ site systems divided in half. The vertical lines depict the value of interaction at which the lowest 50 eigenvalues λ_α are evenly degenerate. The shaded region depicts the topologically trivial phase.